Earthquake location using a 3D velocity model: An example in Sichuan Province, China

by

Carolynn E. Vincent

Submitted to the Department of Earth, Atmospheric, and Planetary Sciences
in partial fulfillment of the requirements for the degree of

Master of Science in Earth and Planetary Sciences

at the

MASSACHUSETTS INSTITUTE OF TECHNOLOGY

September 2000

Author .....
Department of Earth, Atmospheric, and Planetary Sciences
July 28, 2000

Certified by .....
M. Nafi Toksöz
Professor of Geophysics
Thesis Supervisor

Accepted by .....
Ronald Prinn
Chairman, Department of Earth, Atmospheric, and Planetary Sciences

Earthquake location using a 3D velocity model: An example in Sichuan Province, China

by

Carolynn E. Vincent

Submitted to the Department of Earth, Atmospheric, and Planetary Sciences
on July 28, 2000, in partial fulfillment of the
requirements for the degree of
Master of Science in Earth and Planetary Sciences

Abstract

We investigate the benefits of applying three-dimensional velocity models to seismic event location. We develop a technique for three-dimensional seismic event location, utilizing a finite difference method for travel time calculation and a grid search method for location. We apply this technique to the location of three events in Sichuan Province, China, an area of complex deformation and scattered seismicity. The lateral differences between published event locations and those obtained using this three-dimensional technique are between 6.2 and 12.8 km, suggesting that the relocation of a larger number of events may refine our understanding of deformation in this region. The locations using the three-dimensional velocity model compare favorably with locations using a one-dimensional model, returning location depths consistent with the geology of the area and showing smaller location variability when using a jackknifing technique.

Thesis Supervisor: M. Nafi Toksöz
Title: Professor of Geophysics

Acknowledgments

Thanks and appreciation go to Dan Burns, Chuck Doll, Margaret Edie, Michelle Johnson, Jim Lewkowicz, Delaine Reiter, Shirley Rieven, Bill Rodi, Youshun Sun, Nafi Toksöz, Susan Turbak, and Zhenya Zhu. Love and thanks to Mom, Dad, Mimi, Stephen and Christopher.

Contents

List of Figures

Chapter 1

Introduction

Improving the accuracy of seismic event location is an important part of refining tectonic interpretation. Event locations are an important factor in delineating faults, and therefore mislocations can significantly distort our understanding of earth structures. One successful approach to improving event location is the application of three-dimensional seismic wave velocity models to the process.

The impact of three-dimensional velocity models on tectonic interpretation can be seen in the case of the Parkfield segment of the San Andreas fault. In this area, events were mislocated parallel to the fault, which led researchers to believe that it was not vertical, but had a dip. Using a three-dimensional velocity model (Eberhart-Phillips and Michael, 1993), these events where relocated such that they correspond more closely to the surface trace of the fault, greatly reducing the calculated dip of the fault.

For this thesis, we have chosen a region in Sichuan Province, China (figure 1-1) where earthquake locations are widely distributed and do not clearly delineate faults (figure 1-2). We will investigate whether an accurate three-dimensional velocity model of this area will improve the accuracy of earthquake locations and provide better identification of active faults. A three-dimensional model is developed on the basis of previous geophysical and geological studies. Then, three events are relocated using both one-dimensional and three-dimensional models, demonstrating the potential importance of a three-dimensional approach in this area. Figure 1-3 shows the

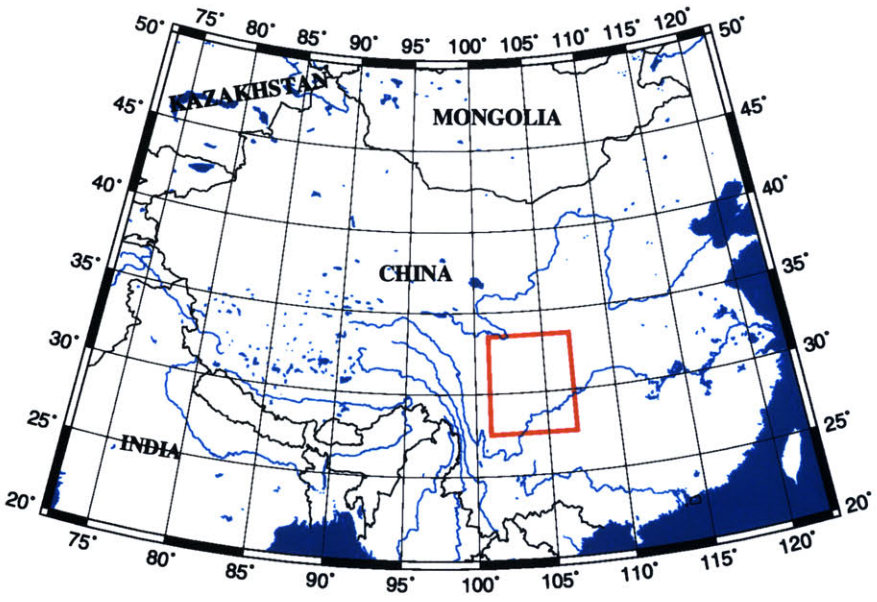

Figure 1-1: Location of study region (red box).

approximate location of the sample events and station coverage.

1.1 Tectonic Setting

The Sichuan study region, which includes Sichuan Province and surrounding areas, is located in the southwestern part of China. Western China can be divided into two main tectonic units, the North China and South China blocks. These blocks collided in late Triassic time and are now delineated by the Qinling suture zone. The South China block (also known as the Yangtze block) can be further divided into the sub-blocks Yangtze I and II (figure 1-4). Yangtze I is a triangular block making up the northwest of the South China block, with Yangtze II making up the southeast of the South China block. According to Kimura *et al.* (1990), the Yangtze I block, on which Sichuan Province is located, was underthrust to the west during Jurassic to Cretaceous time and formed the Sichuan Basin. Small underthrusting also occurred on the eastern and northern borders of the block. The Yangtze I block has

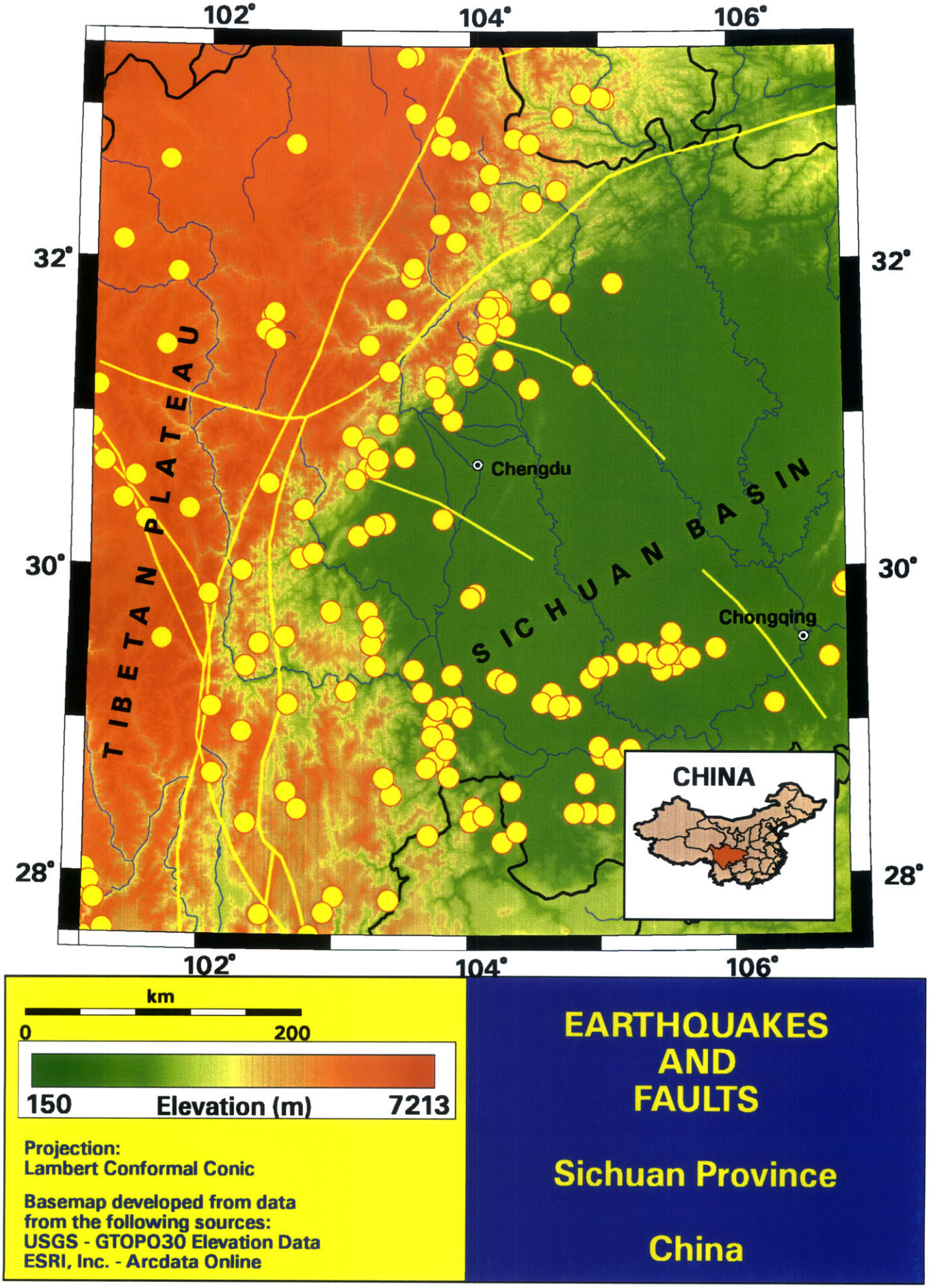
102°
104°
106°
32°
30°
28°
TIBETAN PLATEAU
SICHUAN BASIN
Chengdu
Chongqing
CHINA
km
0
200
150
Elevation (m)
7213
Projection:
Lambert Conformal Conic
Basemap developed from data
from the following sources:
USGS - GTOPO30 Elevation Data
ESRI, Inc. - Arcdata Online
EARTHQUAKES
AND
FAULTS
Sichuan Province
China

Figure 1-2

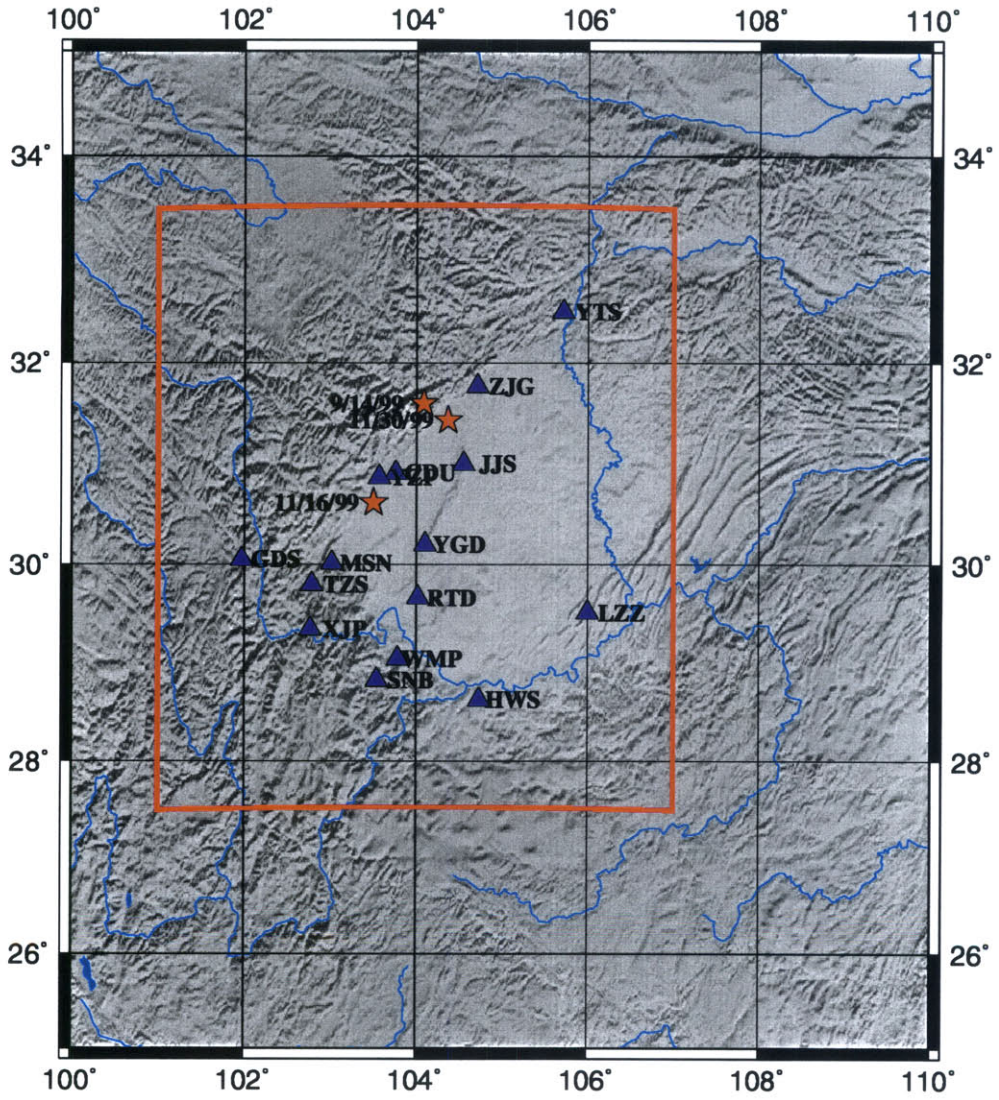

Figure 1-3: Approximate locations of events and station coverage. The red box shows the region covered by the three dimensional velocity model. Stars represent the three events to be relocated, triangles represent station locations.

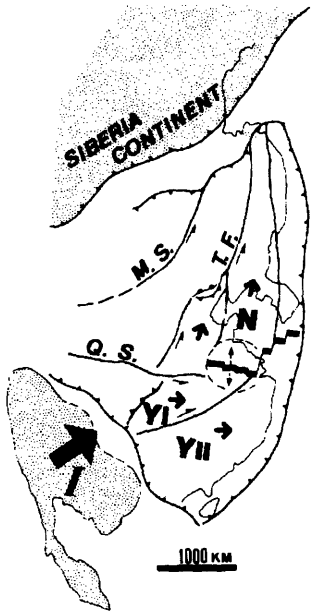

Figure 1-4: Generalized tectonic map of southwestern China, from Kimura *et al.* (1990). Q.S. = Qinling suture zone; N = North China Block; Y I= Yangtze I block; Y II= Yangtze II block: I = Indochina block.

a complicated deformational pattern resulting from its eastward movement relative to the North China and Yangtze II blocks. The collision of India with Asia and the continued northward movement of the Indian plate controls the present day tectonics of Sichuan Province and the surrounding regions (Burchfiel *et al.*, 1995).

This complex tectonic setting makes three-dimensional modeling of the area especially relevant. Two important factors in modeling this area are varying sediment layer thickness and varying crustal thickness. Overall, the Sichuan Basin has a thick sediment layer relative to the rest of the region. The depth to the Moho under the region (figure 1-5) also changes considerably. The depth varies from 40 to 63 km over a 600 km lateral distance, with a general deepening to the west, reflecting the underthrusting of the Yangtze I block (Ren Jishun *et al.*, 1987).

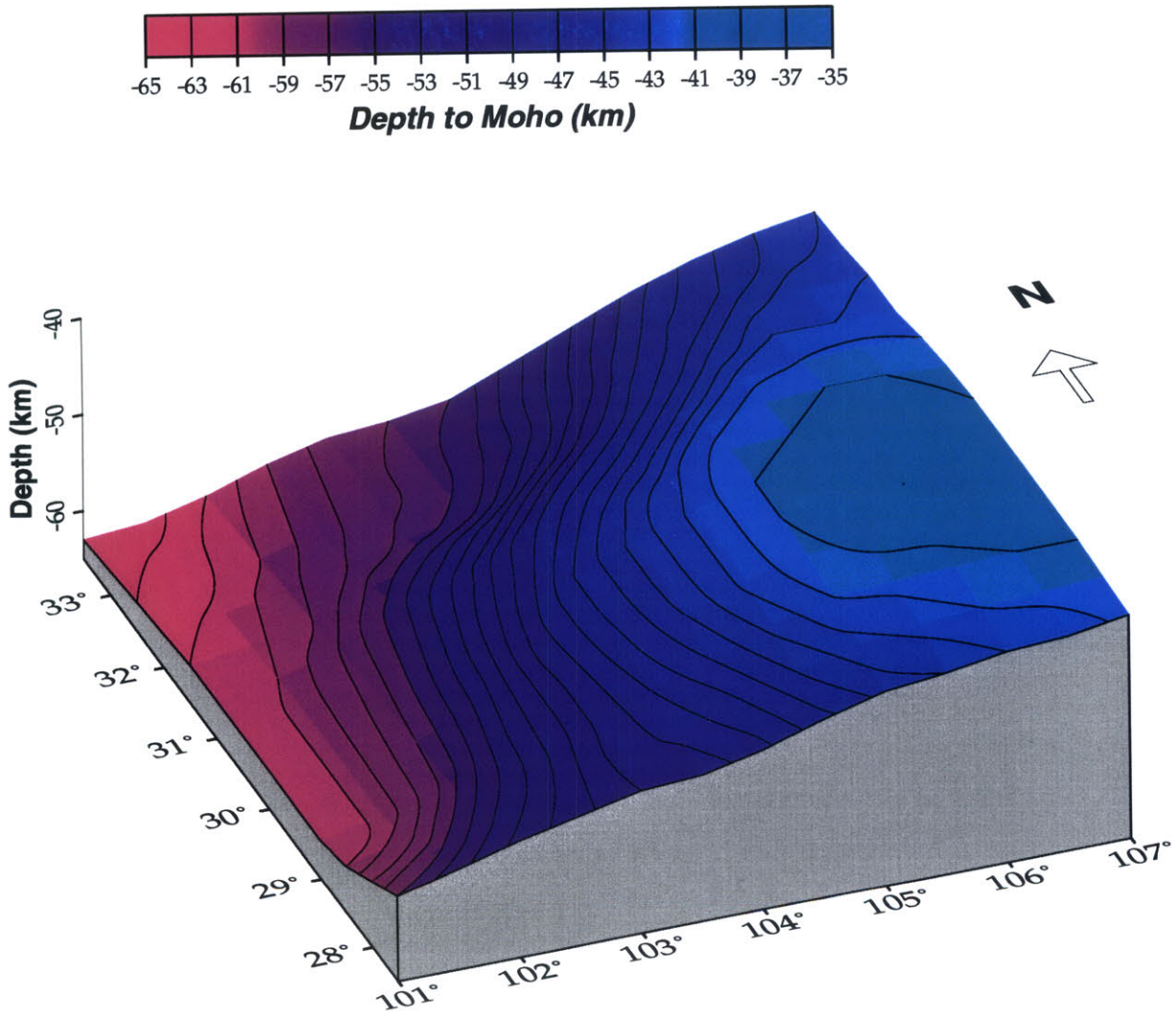

Figure 1-5: Map of depth to Mohorovičić discontinuity for study region. See chapter 2 for sources.

1.2 Overview

Our main goals are to develop a technique for three-dimensional seismic event location and to apply this technique to three events in Sichuan Province. In Chapter 2 we discuss general problems in developing a regional velocity model, then refine these discussions as applied to modeling the Sichuan study area. Earthquake location in three dimensional media including location techniques, finite difference ray tracing, and the application of the procedure to the Sichuan Province are discussed in Chapter 3. In Chapter 4 we present location results for three seismic events, as well as for several synthetic events. Finally, in Chapter 5 we discuss how these locations may change our interpretation of tectonics in the region.

Chapter 2

3D Velocity Model

Compiling a velocity model from heterogeneous data sources and formats is a complex process. Relevant data tends to be available in a number of different representations, including one-dimensional velocity profiles and regional models, two-dimensional velocity cross-sections, two-dimensional velocity slices at fixed depth, Pn velocity maps, general sediment velocity information, and depth to Moho maps. A single format for velocity information is needed in order to combine these different sources, methods of presentation, and scales into a reasonable model of the Earth.

2.1 Velocity Model Format

The general velocity model developed here is made up of one-dimensional velocity profiles spaced every 0.5 degrees in latitude and longitude. Each velocity profile is broken into 5 km constant velocity blocks in depth. The Moho depth is rounded to the nearest 5 km so that the velocity profile does not represent an average of the velocity contrast across the Moho. The actual depth to Moho is stored separately. From this format, velocity can be re-sampled at a finer spacing as required by the ray tracer. The final model input to the raytracer is made of over 2 million 2.5 km voxels, 238 in longitude, 270 in latitude and 41 in depth. See appendix A for more detail on how the model is re-sampled. An S velocity model is calculated assuming a Poisson ratio of 0.25 (S velocity equals P velocity times $\sqrt{3}$).

2.2 Sichuan Model

A three-dimensional velocity model was complied using the following regional and local velocity studies: crustal velocity profiles by Li and Mooney (1998) constructed from deep seismic sounding data, crustal velocity profiles derived from explosion data using two-dimensional raytracing by Yin Zhou-xun and Xiong Shao-bai (1992) and by Xiong Shao-bai *et al.* (1993), and two-dimensional velocity slices from Liu Ruifeng *et al.* (1993) and Zeng Rongsheng *et al.* (1992) which were derived from tomographic inversion of local and teleseismic earthquake data. Figure 2-1 shows the lateral coverage of these studies. Larger studies covering wide sections of the Chinese continent were also incorporated including two-dimensional velocity images by Li Fu-Tian *et al.* (1990) derived from P wave travel time residuals of regional and distant earthquakes, Pn travel times from McNamara *et al.* (1997) obtained by travel time tomography, and a regional velocity profile derived from waveforms and travel times of long period P waves in the upper mantle by Wang Kai and Yao Zhen-xing (1991). Where velocity studies overlap, there are often great discrepancies. In these cases the more local studies are favored. When conflicting numbers are from similarly sized studies, the most conservative numbers are used.

General information on sediment thicknesses and velocities was obtained from Ren Jishun *et al.* (1987) and Ou and Deng (1995) who used a combination of two- and three-dimensional seismic surveys to study the Sichuan basin sediments. The sediment data is not as detailed as was hoped. For this reason, all sediment information used in the model is on the conservative side, with sediments no thicker than 5 km and sediment velocities ranging from 4.6 to 4.8 km/sec. Depth to Moho data from Wang Shangwen (1983) and Ren Jishun *et al.* (1987) was also utilized in building the velocity model.

Figure 2-2 shows two smoothed cross-sections of the resulting velocity model. Two one-dimensional velocity models of the area are provided for comparison. Figure 2-3 shows a one-dimensional model by Li and Mooney (1998) for the Sichuan Province region (figure 2-1 shows the location of this study) developed from bole-hole explosion

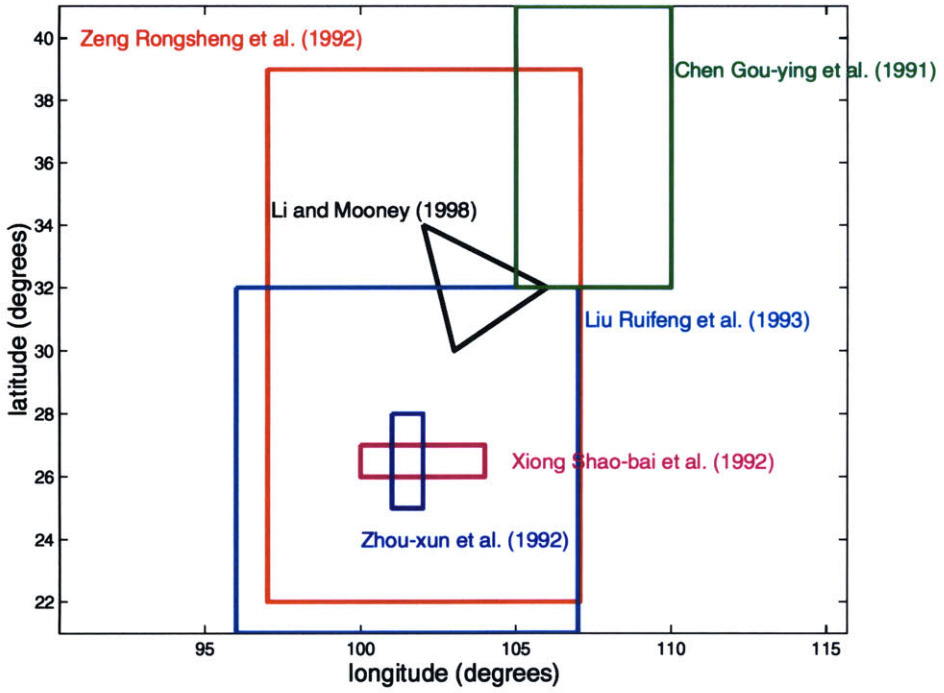

Figure 2-1: Coverage of regional velocity studies.

data and a one-dimensional, six layer model for western Sichuan by Ran Zhou *et al.* (1995) based on travel-time data from local and regional earthquakes.

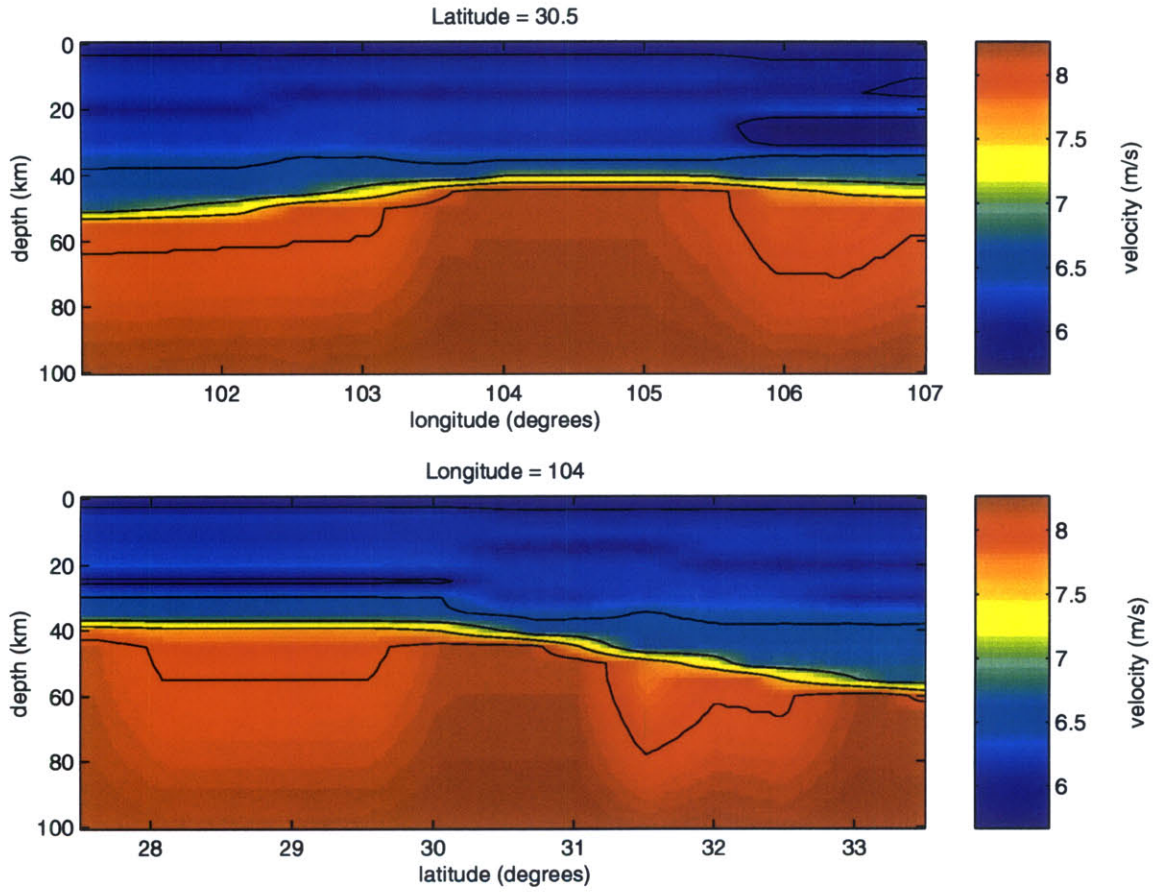

Figure 2-2: Cross-sections of three-dimensional velocity at 30.5 degrees latitude (top) and 104 degrees longitude (bottom).

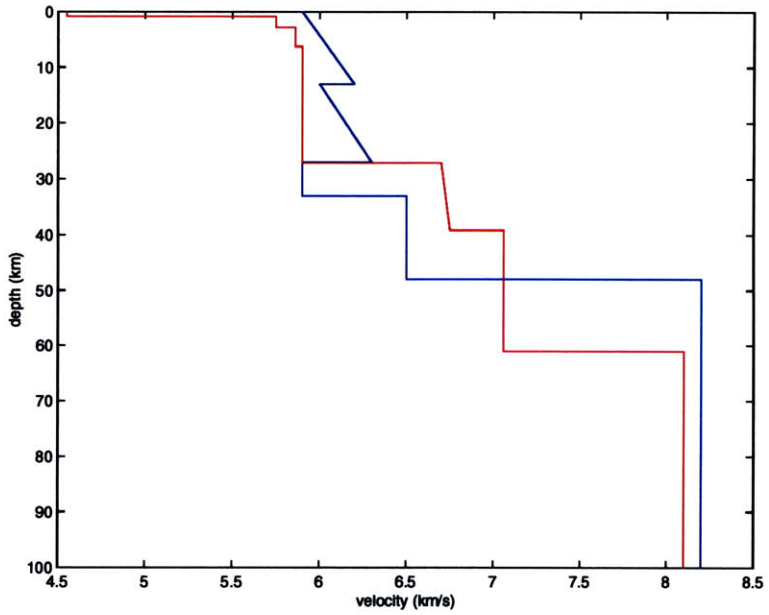

Figure 2-3: One-dimensional velocity models of the Sichuan study region. From Mooney and Li (1998), blue profile and the six layer model from Ran Zhou et al. (1995), red profile.

Chapter 3

Earthquake Location in 3D Media

A number of computational methods have been applied to A number of computational method methods have been applied to earthquake location, we outline and compare several popular approaches. Earthquakes have traditionally been located using one-dimensional velocity models. Flinn (1965) implemented the least squares Geiger's method (Geiger, 1910) for locating events and developed a method for calculating confidence regions. Julian and Gubbins (1977) discuss two methods of two point ray tracing, bending and iterative shooting. Both methods can be used with three-dimensional velocity models. Shooting is an initial value problem where the takeoff parameters are initially estimated, then refined over several iterations. Bending is a two point boundary value problem where an estimate of the ray path between two points is successively refined until it becomes stationary. Um and Thurber (1987) developed a bending method which minimizes travel time rather than solving the ray equation. These methods all calculate travel times as they are needed in the location process.

More recently, various searches of travel time tables has been used for earthquake location. Here a table of travel times is needed before the location process can begin. Sambridge and Kennett (1986) developed a directed grid search method which minimized a misfit function based on travel time residuals. Dreger, *et al.* (1998) implemented a grid search routine which searches grids of increasing fineness as the search is narrowed. Sambridge (1999) introduced a method of searching a parameter

space, such as a set of travel time tables, which preferentially focuses on regions of good data fit.

3.1 GSEL

Our approach utilizes GSEL (Grid Search Event Location), an algorithm developed by Rodi (personal communication, 2000) for locating events using a three-dimensional model. GSEL minimizes the norm of travel time residuals by maximizing a likelihood function based on the joint probability density function of the arrival time data. It searches a grid of hypocenters consisting of a set of subgrids of increasing fineness. The finest grid has a spacing of approximately 0.3 km, such that GSEL finds the least-square hypocenter to within 0.3 km.

3.2 Finite Difference Ray Tracing

GSEL operates on a set of travel time tables generated for three-dimensional earth models. These tables could be calculated through a large number of ray bending or shooting algorithms or using a finite difference ray tracing method. Vidale (1980) developed a finite difference method for calculating travel times which tracks wavefronts through a three-dimensional model by solving the eikonal equation of ray theory. This method, given a reasonably smooth model, accurately calculates propagation, including head waves and diffracted waves. Moser (1991) developed a different method for calculating travel time tables which uses a graph search method for finding the minimum time ray paths.

Travel times for this study were calculated using the NonLinLoc algorithm (Lomax, 2000), which implements the wavefront tracing method of Podvin and Lecomte (1991). This method applies Huygens' principle in the finite difference approximation, correctly accounting for different modes of propagation. Podvin and Lecomte demonstrated that this approach produces accurate first arrival travel times from velocity models with extreme and arbitrarily shaped velocity contrasts.

3.3 Application to Sichuan Province, China

Before using GSEL to locate events, travel time grids were calculated. The first step in doing that was choosing grid spacing for the finite difference algorithm. The accuracy of finite difference calculations is proportional to the density of the grid on which the times are calculated. Decreasing the spacing between grid points increases the accuracy but must be balanced with increasing data size and limits on computer memory. Figures 3-1 shows the travel time error in a homogeneous model at 10, 5, 2.5, and 1 km grid point spacings. Since this is a finite difference method, there are variations in accuracy depending on how well the ray path can be fit by the finite difference scheme. The most accurate times are calculated for ray paths that correspond to a straight line of nodes, either along grid cube edges, corner to corner through grid cubes, or corner to corner on a cube side. For application to the Sichuan model, we chose a 2.5 km spaced grid which yields a 0.27 second maximum error for a homogeneous medium over a region similar in size to the Sichuan study region. The travel time error is smaller than the picking error for the earthquake arrivals data. The finer 1 km grid is not used because files becomes prohibitively large.

The velocity model discussed in Chapter 2 uses spherical coordinates and must be converted to a Cartesian grid as required by the ray tracer. This is done with an emphasis on preserving distance and requires separate velocity grids for each station. See Appendix B for more information on this conversion. A flattening correction is applied to the velocity model to account for curvature of the Earth. Flattening corrections are discussed in Appendix C.

Travel times were calculated for all the stations. An example of the effect of the three-dimensional velocity model on travel times can be seen in figure 3-2. Figure 3-2 shows the difference in seconds between the travel times at the surface calculated from the three-dimensional model and the one-dimensional six layer model (figure 2-3) for station YTS. Near the source, there is only a small difference in travel times. Further distances, however, show differences up to 2.6 seconds which corresponds to a distance of more that 15 km. The ring approximately 150 km from the source is a

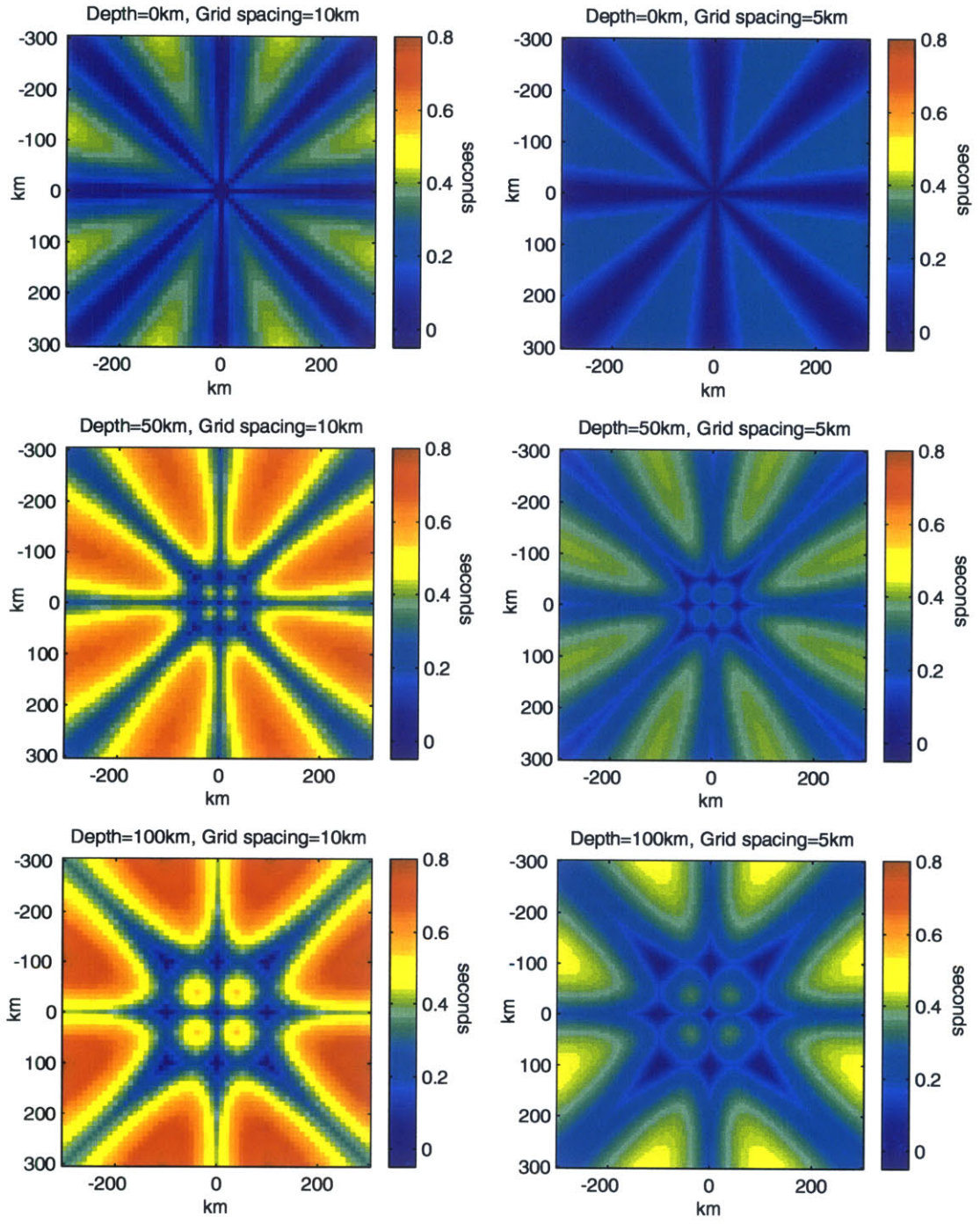

Figure 3-1: Accuracy of finite difference calculations.

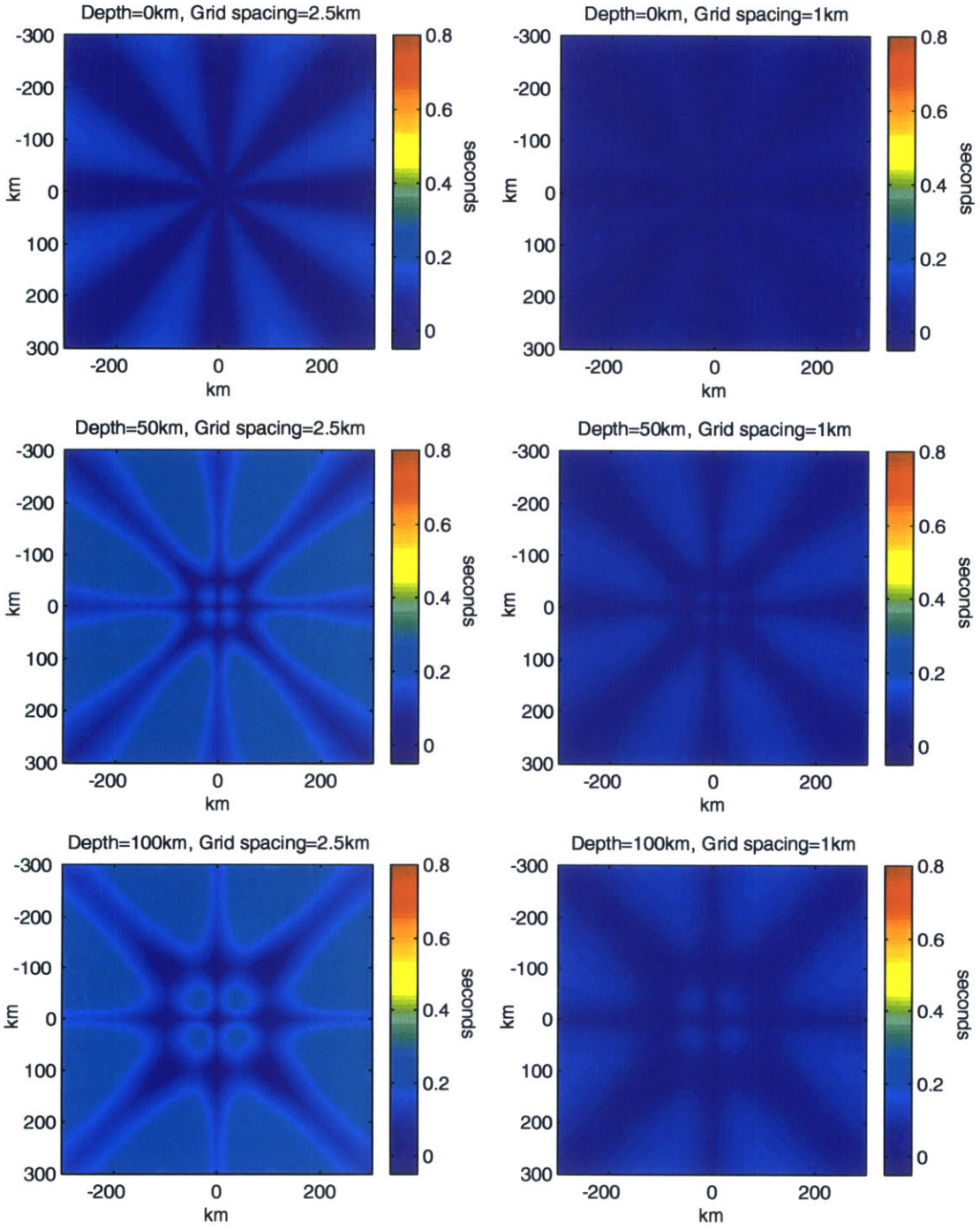

Figure 3-1: Cont'. Accuracy of finite difference calculations.

result of different Pn crossover distances for the two models, due primarily to different Moho depths.

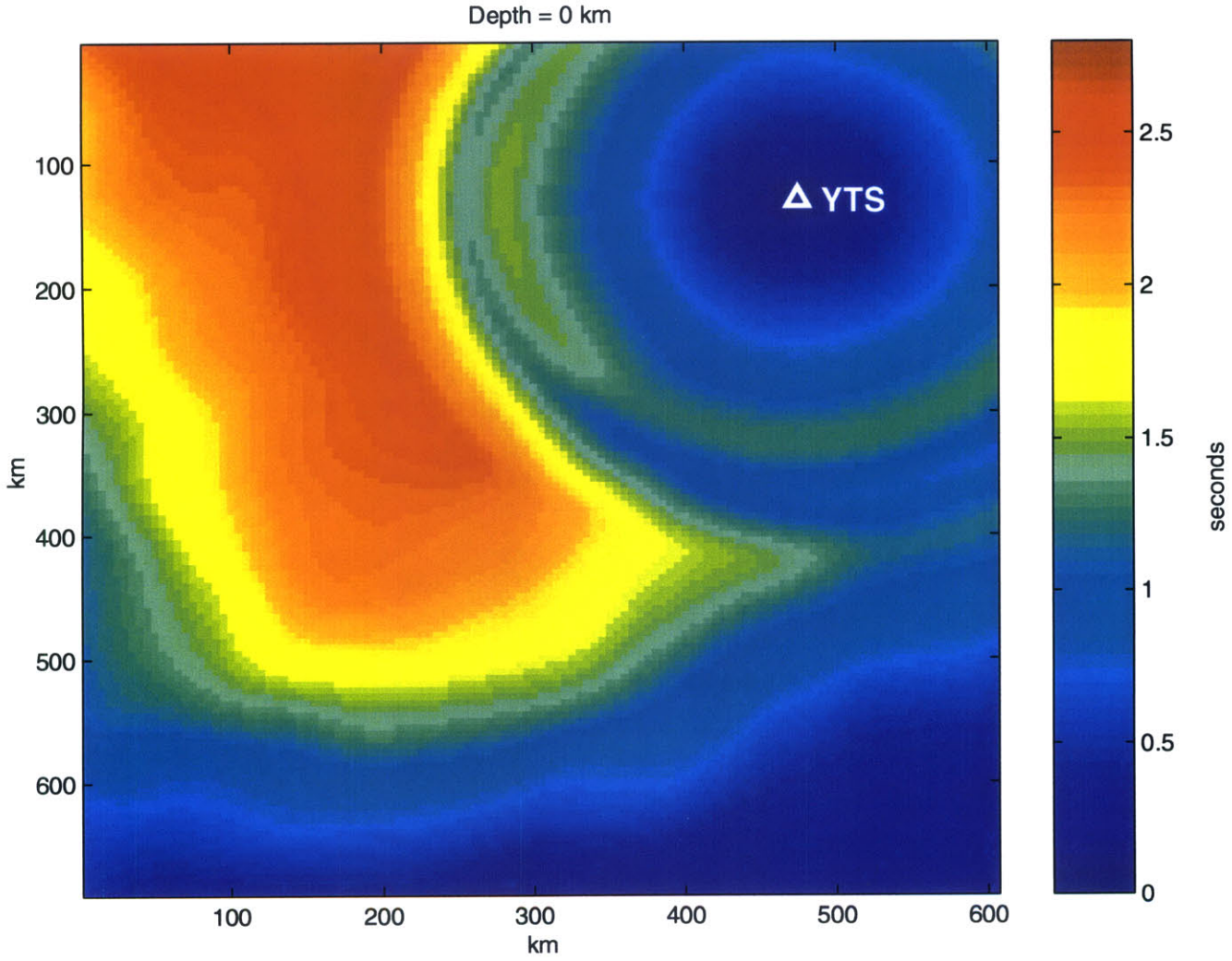

Figure 3-2: Difference in travel times calculated using the one-dimensional six layer model shown in figure 2-3 (Ran Zhou *et al.*, 1995) and the three-dimensional velocity model of the Sichuan study region shown in figure 2-2 for station YTS.

Chapter 4

Location Results

Several synthetic events are generated. Locations are then computed using the one-dimensional six layer layer model (Ran Zhou *et al.*, 1991; see figure 2-3) and compared with locations generated by the three-dimensional model. Three real events are locate using both the one-dimensional six layer model and the three-dimensional model. Special attention is paid to the influence of S waves on location and the substantial differences in depth between the one- and three-dimensional model locations in both the synthetic and real cases. The Grid Search Location (GSEL) algorithm is used to compute all locations. The location capabilities of GSEL are compared with those of a widely used location program, HYPOINVERSE, in appendix D.

4.1 Location of synthetic events

There are gaps in the station coverage for the three real events we will be looking at. For the initial synthetic location tests, the real seismic array of 16 stations is supplemented with 17 imaginary stations to fill in these gaps, bring the total number of stations to 33 (figure 4-1). Arrivals for five synthetic events were calculated using the three-dimensional travel time tables. These five events share the same epicenter at 31.6 degrees longitude and 104.2 degrees latitude, which is in the region of the three real events, and depths of 0, 10, 20, 30, and 40 km. Gaussian noise with a mean of 0.5 seconds was added to the P arrivals, and noise with a mean of 1 second was added to

the S arrivals. Locations were calculated using both the one- and three-dimensional models, using only P arrivals as well as using both P and S arrivals. The resulting location epicenters are shown in figure 4-3 and the location depths are shown in figure 4-2. The locations using the three-dimensional model (blue symbols) are within 2.5 km of the true depth when only the P arrivals are used and within 1.1 km when both the P and S arrivals are used. The locations using the one-dimensional model (red symbols) are between 11.4 and 32.5 km deeper than the true depth when only the P arrivals are used. This result for the one-dimensional model does not improve with the addition of S arrivals which in fact push the location deeper in most cases. These substantial errors in depth are due to the misrepresentation of the Moho in the one-dimensional model. The epicenters for locations using the three-dimensional model are within 1 km of the true epicenter for both the case where only P arrivals are used and the case where P and S arrivals are taken in to consideration. All of these locations are slightly to the East of the true epicenter. For the one-dimensional model locations the epicenters are from 1.2 to 5.2 km away from the true epicenter. These are all mislocated from 0.9 to 1.7 km west of the true epicenter. This is expected because the Moho is approximately 48 km deep at the true epicenter and slopes to the west in the model used to generate the arrival times while the one-dimensional model has a constant Moho depth of 60 km.

The next set of synthetic tests use the same arrival times as in the above mentioned test, however, only the real stations and arrivals observed in the real events are used. This includes P arrivals at 14 real stations (real stations are shown in red in figure 4-1) and in some cases S arrivals at four of these stations (CDU, GDS, YGD, and YTS). Locations were again calculated using both the one- and three-dimensional models, using only P arrivals as well as using both P and S arrivals. The resulting location epicenters are shown in figure 4-4 and the location depths are shown in figure 4-5. The resulting depth component in all cases remains similar to the results seen using the 33 station array. The three-dimensional model location depths are with 2.9 km of the true depth with or without the S arrivals. Using the one-dimensional model, mislocations in depth range from 8.3 to 27.8 km deeper that the true depth. The

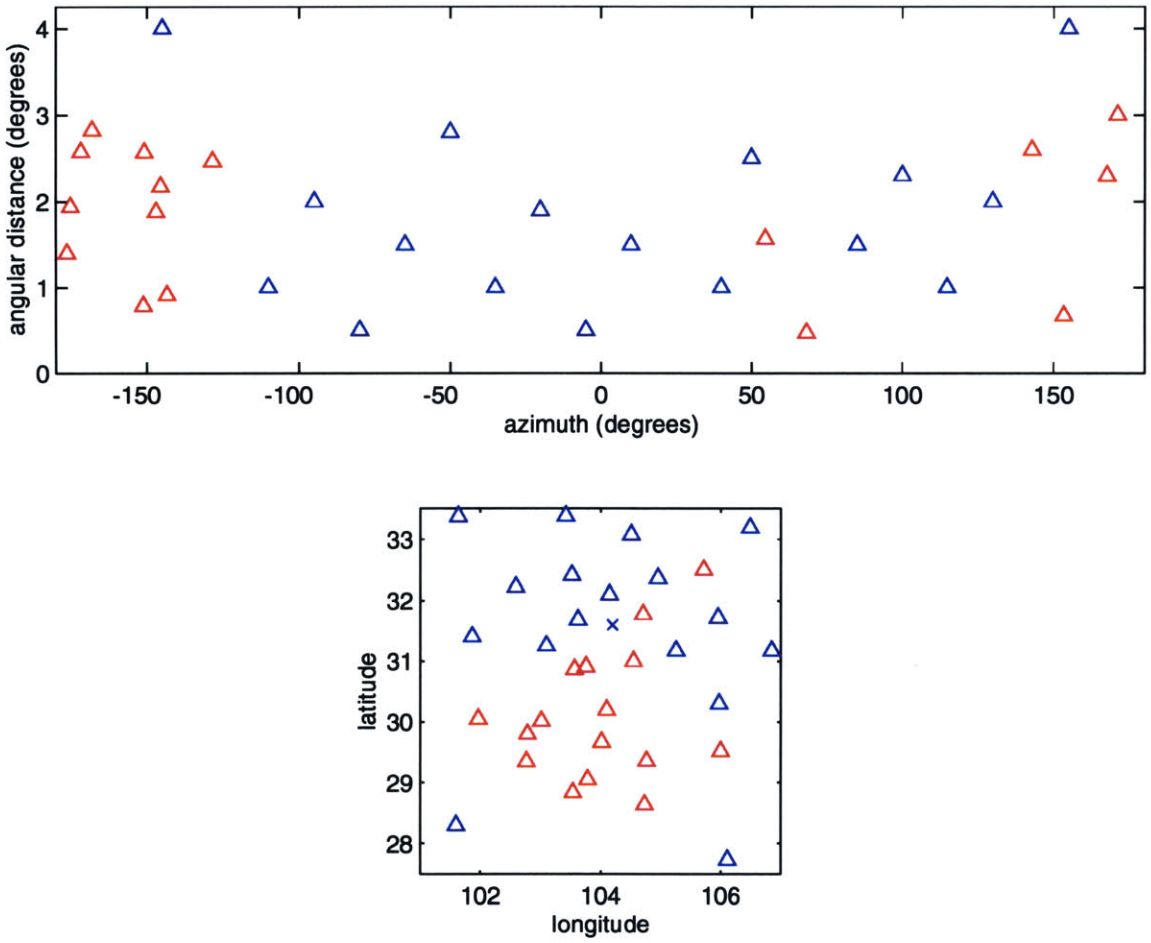

Figure 4-1: Station coverage. The top figure shows station coverage in distance versus azimuth with respect to the location of the synthetic event epicenter. The bottom figure shows the station locations in map view. The red triangles represent the real stations and the blue triangles represent the imaginary stations used to supplement coverage. The green x marks the synthetic event epicenter.

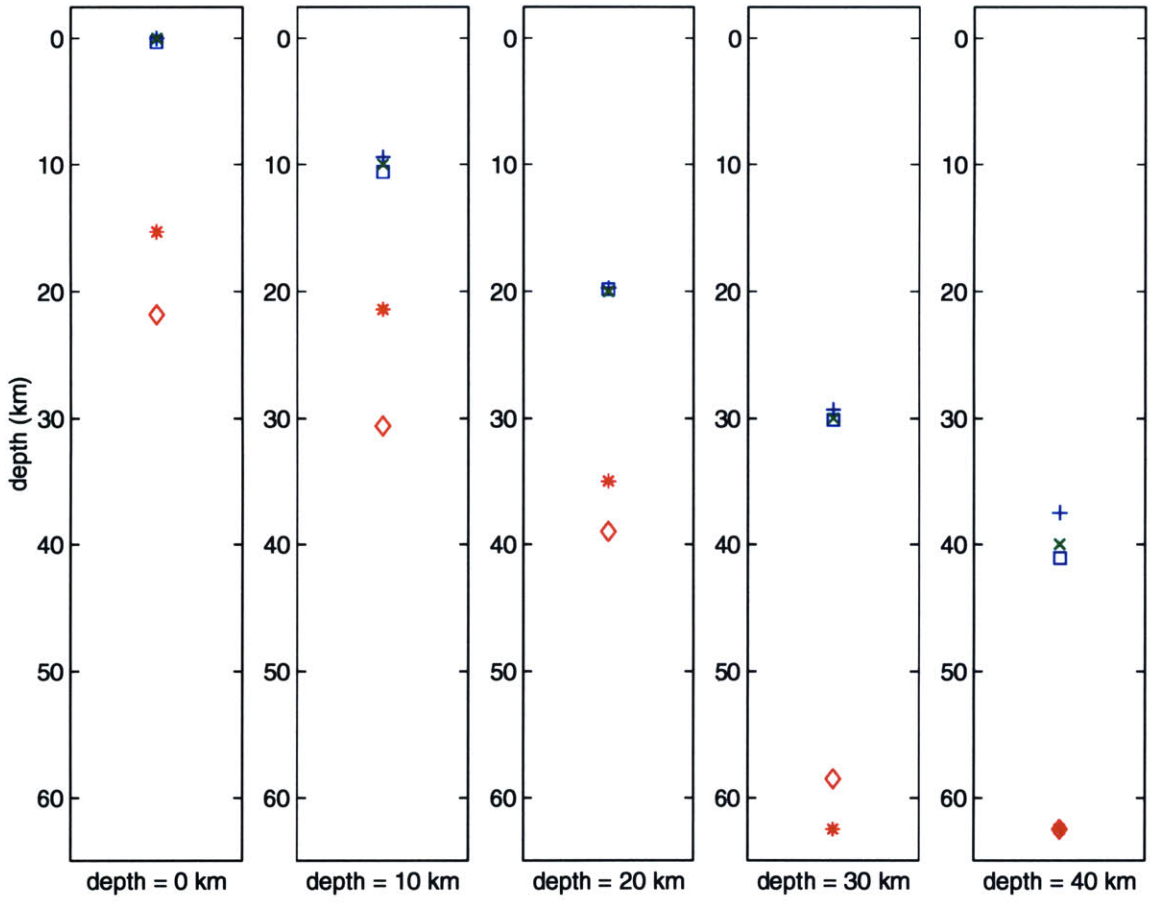

Figure 4-2: Depth component of locations using P and S wave arrivals at 33 real and imaginary stations for synthetic events located, from left to right, at 0, 10, 20, 30, and 40 km depth. Blue +'s denote GSEL locations using the three-dimensional model with only P arrivals, blue squares denote GSEL three-dimensional model locations using P and S arrivals, red *'s denote GSEL locations using the one-dimensional model with only P arrivals, and red diamonds denote GSEL one-dimensional model locations using P and S arrivals.

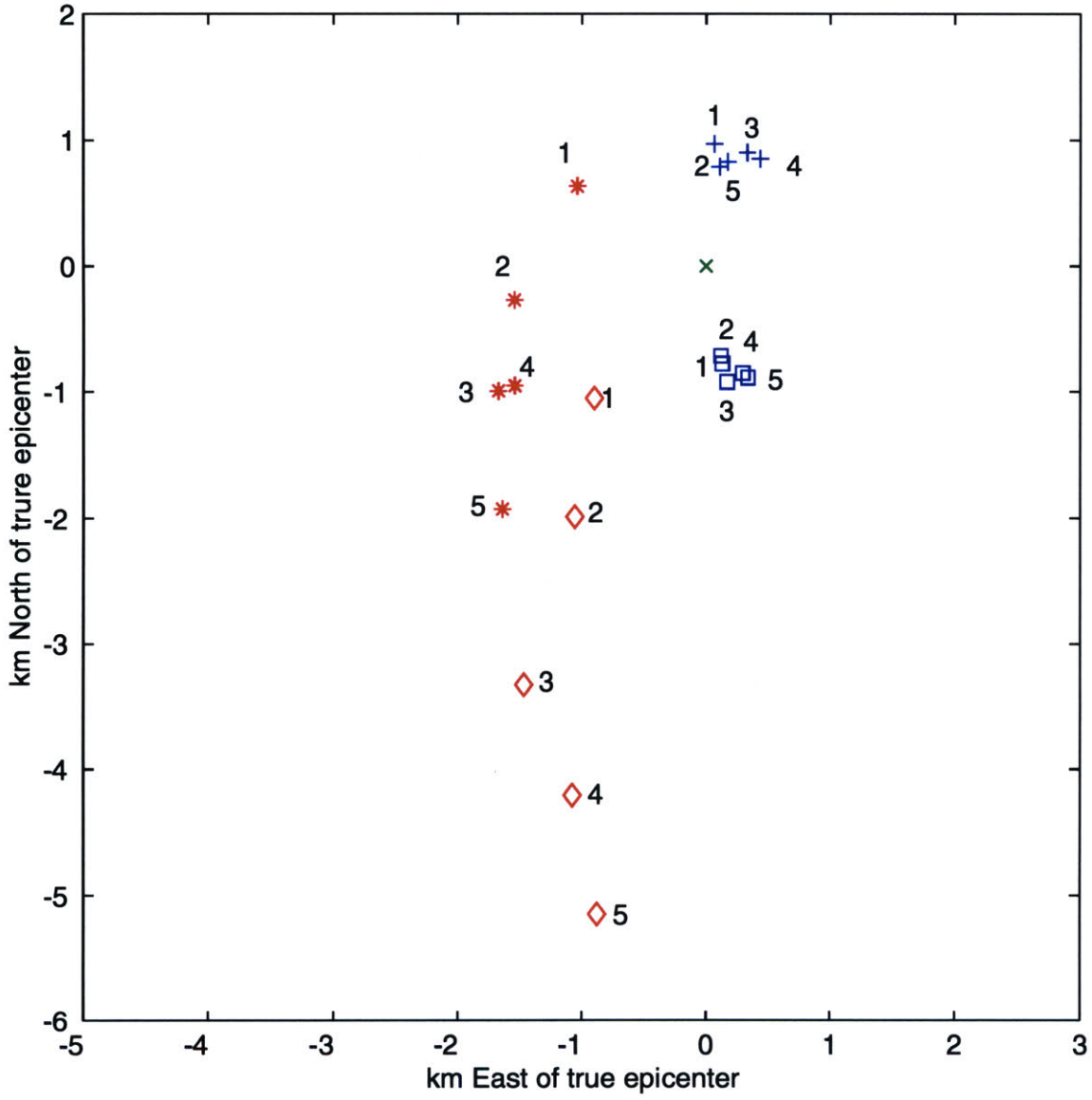

Figure 4-3: Epicenters for synthetic events located using P and S wave arrivals at 33 real and imaginary stations. The green x denotes the true location, the blue + denotes the GSEL location using the three-dimensional model with only P arrivals, the blue square denotes the GSEL three-dimensional model location using P and S arrivals, the red * denotes the GSEL location using the one-dimensional model with only P arrivals, and the red diamond denotes the GSEL one-dimensional model location using P and S arrivals.

calculated epicenters are mislocated to the south of the true epicenter in all cases. This is due to the gaps in the seismic array coverage to the North. However the pattern of east-west mislocation remains similar with all the three-dimensional model epicenters located slightly east of the true epicenter and all the one-dimensional model epicenters mislocated from 0.8 to 3.8 km to the west. The total lateral mislocation ranges from 1.5 to 6 km for the one-dimensional model case and from 2 to 3.5 km in the three-dimensional case.

The largest location errors in all the synthetic tests were in the depth component. The one-dimensional depths were too deep in all case. This confirms that model error can shift location depth significantly.

4.2 Location of three real events

Shown in figures 4-6 and 4-7 are event locations calculated by GSEL using the six layer, one-dimensional model and only P arrivals (red *'s) and the three-dimensional model using only P arrivals (blue +'s) for three real events. The most distinct difference between the locations using the one-dimensional and three-dimensional models is the depth. The one-dimensional model locations are from 15 to 30 km deeper than those for the three-dimensional model. This difference is perhaps even greater, since the depth for the one-dimensional location of event three is 62.5 km depth, resting at the lower extent of the model. When S arrivals are also used for location, the one-dimensional locations (red diamonds) remain much deeper than the three-dimensional locations (blue squares). This pattern of depth locations is similar to the pattern seen in the synthetic examples. The depth component of both three-dimensional locations are near each other and much shallower than the depth components of the one-dimensional locations.

Figure 4-8 shows the depth distribution of seismic events in the Sichuan study area from 1980 to present. Events located using a fixed depth of 33 km have been omitted. The majority of events are located above 40 km, with a large number of events in the 15 to 35 km range, similar to the three-dimensional model locations.

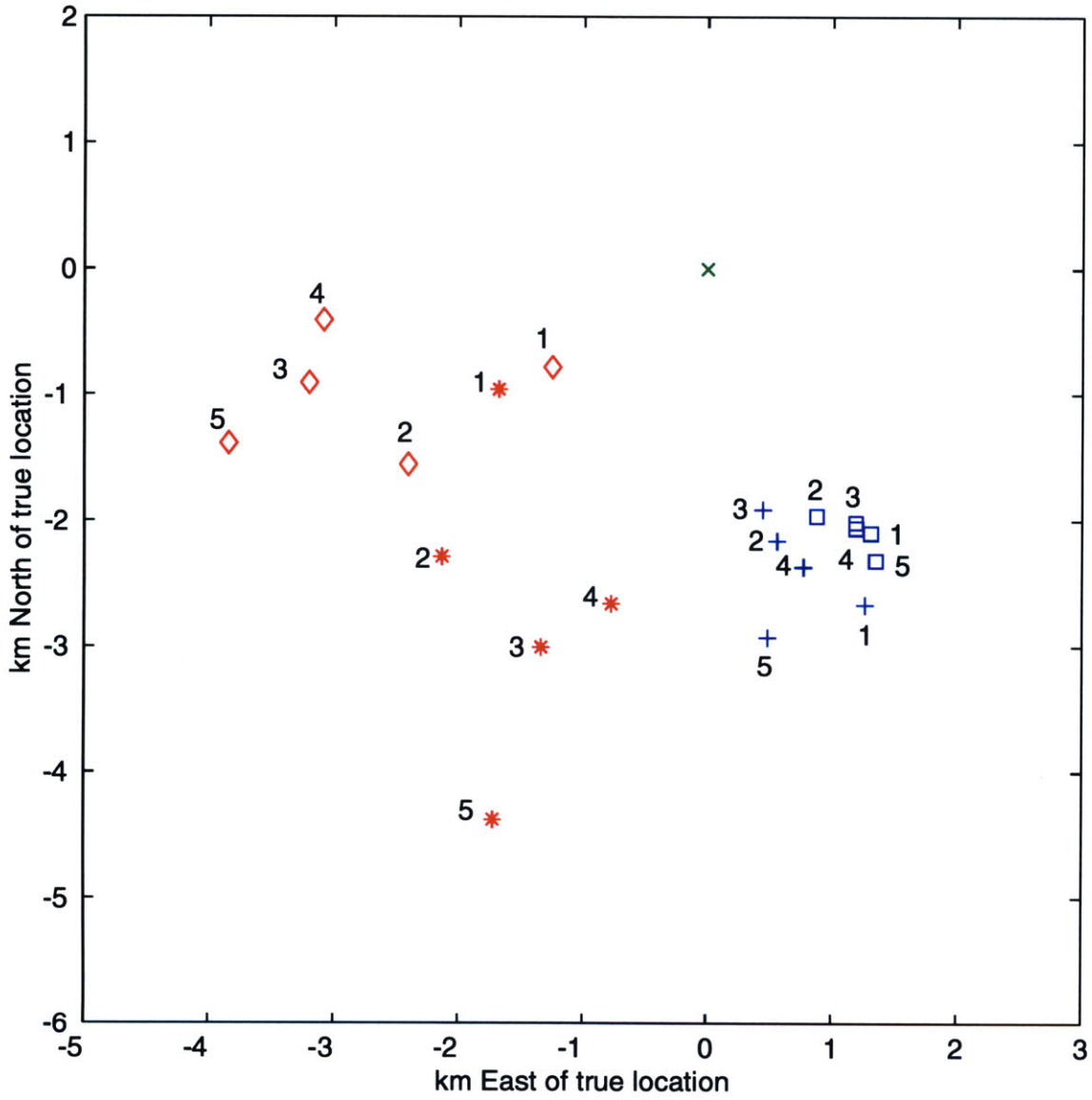

Figure 4-4: Epicenters for synthetic events located using P wave arrivals at 14 real stations and S wave arrivals at 4 of those stations. The green x denotes the true location, the blue + denotes the GSEL location using the three-dimensional model with only P arrivals, the blue square denotes the GSEL three-dimensional model location using P and S arrivals, the red * denotes the GSEL location using the one-dimensional model with only P arrivals, and the red diamond denotes the GSEL one-dimensional model location using P and S arrivals.

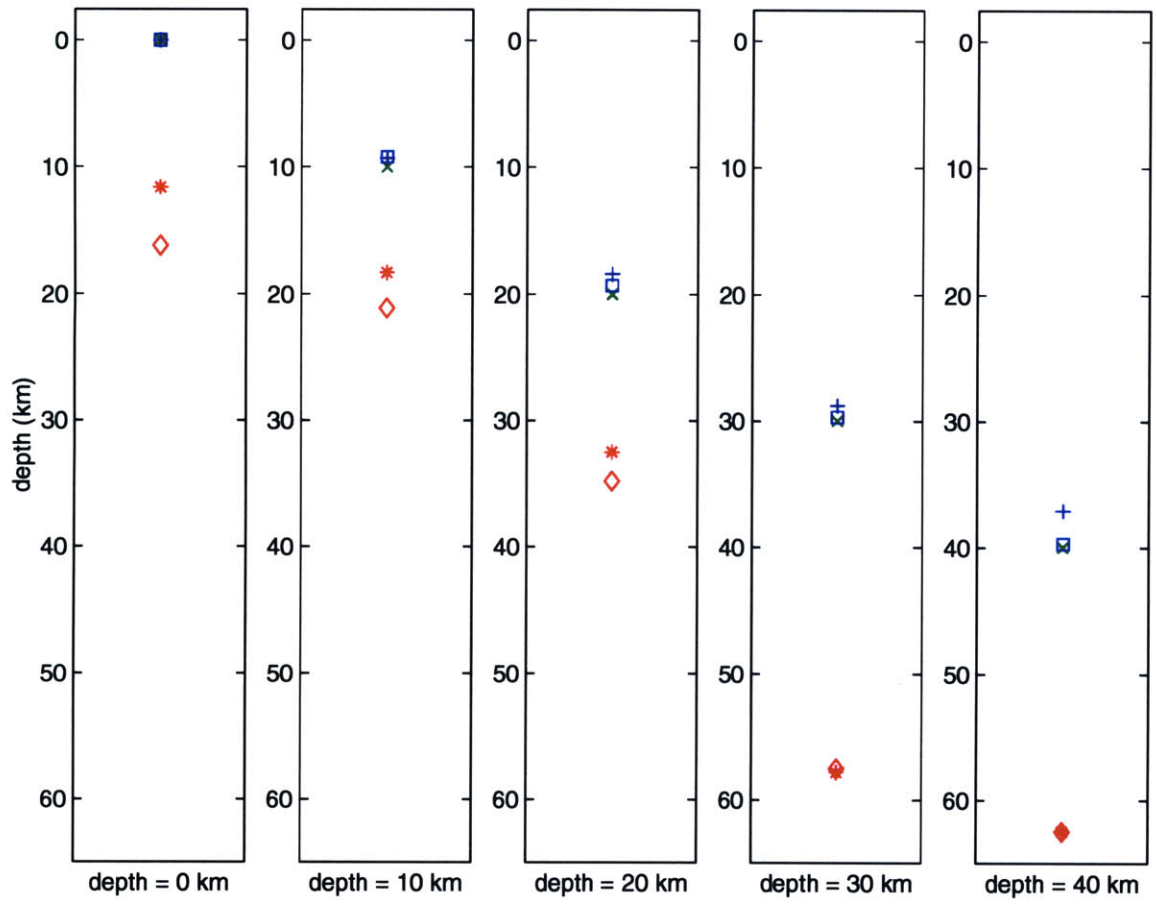

Figure 4-5: Depth component of locations using P wave arrivals at 14 real stations and S wave arrivals at 4 real stations for synthetic events located, from left to right, at 0, 10, 20, 30, and 40 km depth. Blue +'s denote GSEL locations using the three-dimensional model with only P arrivals, blue squares denote GSEL three-dimensional model locations using P and S arrivals, red *'s denote GSEL locations using the one-dimensional model with only P arrivals, and red diamonds denote GSEL one-dimensional model locations using P and S arrivals.

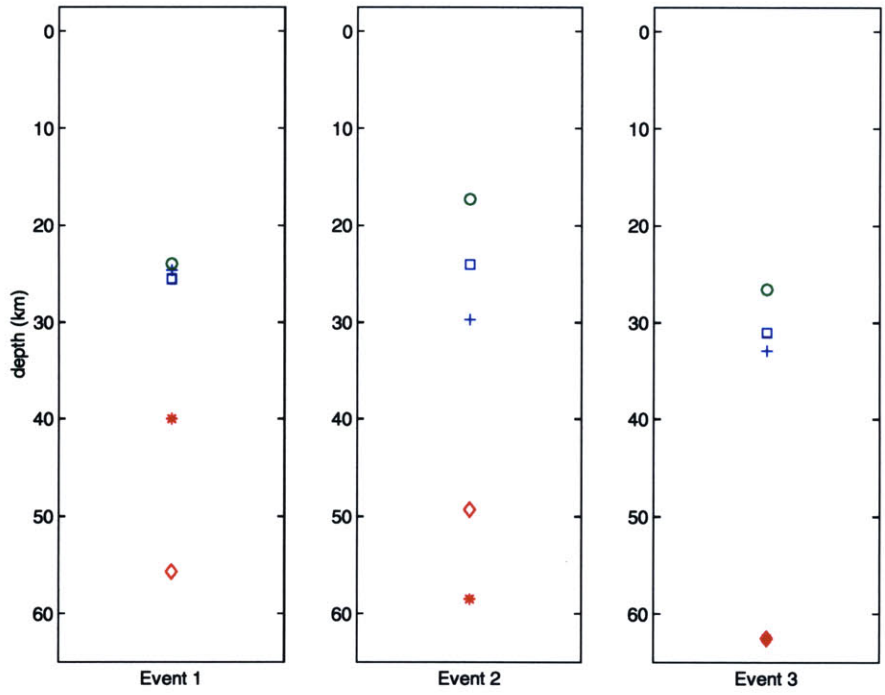

Figure 4-6: Depth component of locations, from left to right, for events one, two, and three. Green circles denote HYPOINVERSE locations, blue +'s denote GSEL locations using the three-dimensional model with only P arrivals, blue squares denote GSEL three-dimensional model locations using P and S arrivals, red *'s denote GSEL locations using the one-dimensional model with only P arrivals, and red diamonds denote GSEL one-dimensional model locations using P and S arrivals.

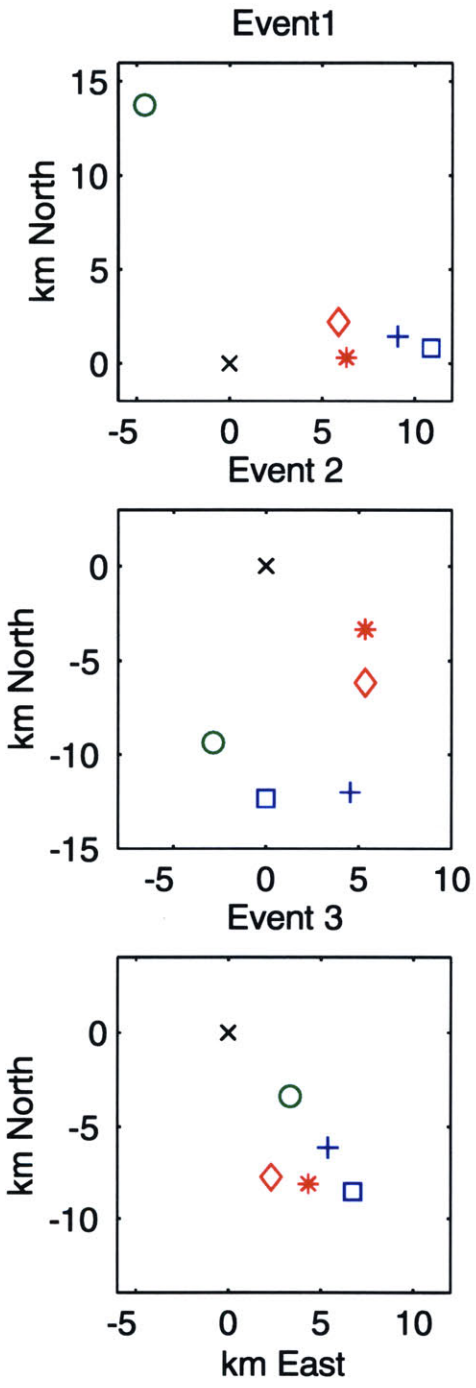

Figure 4-7: Epicenters for events one, two, and three. The black x denotes the published epicenter, the green circle denotes the HYPOINVERSE location, the blue + denotes the GSEL location using the three-dimensional model with only P arrivals, the blue square denotes the GSEL three-dimensional model location using P and S arrivals, the red * denotes the GSEL location using the one-dimensional model with only P arrivals, and the red diamond denotes the GSEL one-dimensional model location using P and S arrivals.

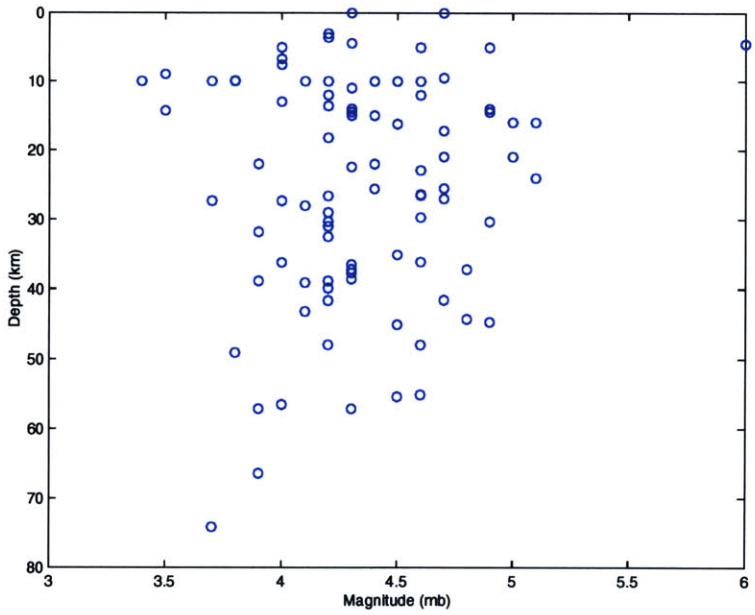

Figure 4-8: Depth distribution of seismic events in the Sichuan study region from 1980 to present. Events located using a fixed depth of 33 km have been omitted

There are very few events in the 50 to 60 km range that the one-dimensional model locations favor.

Figure 4-7 shows how the epicenters of the events move depending on location models. The three-dimensional model locations (blue symbols) tend to be further from the published locations (black x's) than the one-dimensional model locations (red symbols). All of these locations are a significant distance, however, from the published locations, varying from 6.2 to 12.8 km laterally.

4.3 Informal jackknife type error estimate

The jackknife (Efron and Gong, 1983) is a method of estimating standard error. Given a statistic of a data set, the change in that statistic when it is calculated using a subset of the data set is an indicator of the error of the data set. The less the statistic changes when calculated using various data subsets, the smaller the error of that data set. This idea is applied informally to the locations of the three real events. Each event is located a number of times, excluding one station each time.

The average of the difference between each location using a subset of the data and the location using the full data set is calculated. This average is used as an indicator of error, a smaller average indicates that a more appropriate model was used.

Each event was located using the method above, both using the one-dimensional and three-dimensional models. Locations with the three-dimensional model varied less for events one and two compared to results using the one-dimensional model. For event one, the average location change was 2.72 km using the three-dimensional model and 5.74 km using the one-dimensional model. For event two these averages were 5.30 km and 6.34 km. The smaller location variability suggests that the three-dimensional model is more appropriate than its one-dimensional counterpart. For event three the results for the one-dimensional model seem better, with an average location change of 2.33 km using the three-dimensional model and 1.81 km using the one-dimensional model. On closer inspection, however, locations for event three using the one-dimensional model are at the lower depth bound for the crusts (the lower extent of the model) almost half the time. Without this lower depth bound, the average location change for the one-dimensional case would have been larger, however deeper locations are geologically unlikely since this would put the hypocenters below the Moho.

Chapter 5

Conclusions

Three-dimensional velocity models are an important tool for improving event location in geologically complex areas. The relocation of only three events in this region does not provide enough information to make conclusions about fault structure or deformation patterns. However, the lateral change in location for these events, from 6.2 to 12.8 km, is significant. This suggests that relocation of a larger number of events may lead to a refined understanding of the deformation of this region.

Location depths resulting from the three-dimensional velocity model correspond more closely to our geological understanding of the region than those for the same events using the six layer, one-dimensional velocity model. Earthquakes tend to occur in the middle to upper crust instead of near the Moho where material becomes more ductile and less susceptible to faulting. Looking at the location of events in Sichuan, from 1980 to the present, the majority of events are located shallower than the one-dimensional model locations.

Event locations can continue to be improved by refining the three-dimensional velocity model. The incorporation of more local velocity studies and sediment thickness information will be an important part of this process. Another path to model improvement could be through tomographic inversion of travel times, using the three-dimensional model as a starting point and updating it to reduce residuals for a large number of events.

Appendix A

Velocity Model Interpolation

The velocity model is a set of velocity profiles, spaced every 0.5 degrees in x and y, and an exact Moho depth for each of those points. Each profile is made up of a set of velocities which are sampled every 5 km in depth. Each velocity represents the average velocity for a given 5 km section in depth. For example, the first velocity in each profile represents the average velocity from 0 km depth to 5 km depth. The Moho is rounded to the nearest 5 km such that the velocity contrast across it is preserved.

To begin the resampling process, the exact depth to the Moho is bilinearly interpolated for each new point of interest. The following formula is used for the interpolation:

$$X = (a) * (b) * A + (1 - a) * (b) * B + (a) * (1 - b) * C + (1 - a) * (1 - b) * D \quad \text{(A.1)}$$

where A, B, C, and D are the data values at the four nearest points, X is the value at the new point, and a and b represent the distance of X from it's nearest neighbors (fig A-1).

This Moho depth is then used to 'stretch' and 'shrink' each of the four nearest velocity profiles so that their Moho depths are aligned with that of the new point (figure A-2 (2)). Then, the new velocity profile is calculated through bilinear interpolation

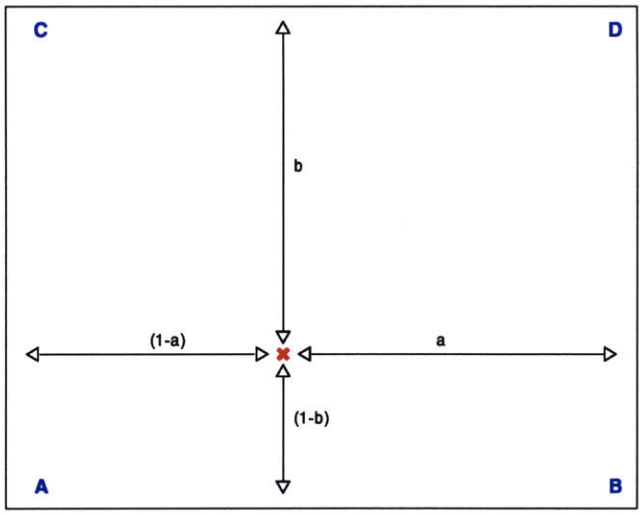

Figure A-1: Bilinear interpolation of data at point X uses the values at points A, B, C, and D weighted by the relative distance of X from each of them.

of the adjusted velocity profiles (figure A-2 (3)).

Through this process, the velocity contrast across the Moho is not smeared over several velocity blocks. At most, one velocity in each profile represents a combination of crustal and mantle velocities. If bilinear interpolation were used without the 'stretch/shrink' step, in areas where the depth of the Moho changes dramatically the interpolated velocity profiles would not have a sharp velocity contrast across the Moho (figure A-2 (4)). Instead the velocities near the Moho would be an average of crust and mantle velocity values.

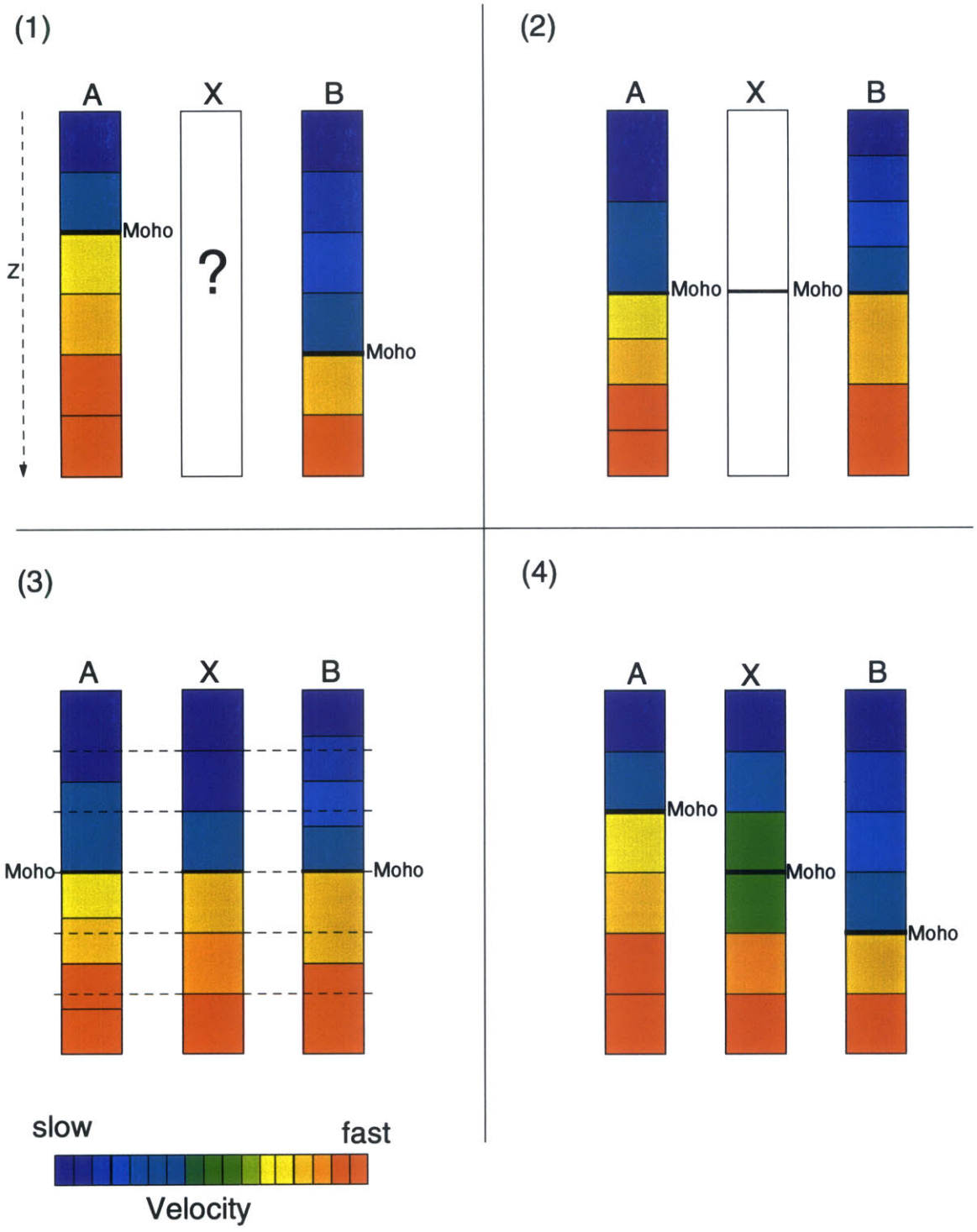

Figure A-2: The 'Stretch' and 'Shrink' of velocity profiles for interpolation. In panel 1, the depth to Moho at X is interpolated from the depths at A and B. Panel 2 illustrates the 'stretching' and 'shrinking' of profiles A and B so that all the Moho depths line up. Finally, in panel 3, the velocities for profile X are interpolated from profiles A and B. Note that the velocity contrast across the Moho is preserved. Panel 4 illustrates the lost of velocity contrast across the Moho when simple interpolation is used.

Appendix B

Velocity Model Conversion

Converting the velocity model from a spherical to a Cartesian system causes some distortion of the model geometry. To minimize the impact of this distortion on travel time calculations, special attention is paid to preserving lateral distance between points.

For a given station, the distance from it to any point in the Cartesian grid should be as close to the distance from the station to the same point in the spherical model. A simple conversion of degrees to kilometers using a constant is not adequate since kilometers per degree varies with latitude. Instead, the distance and azimuth from the station to a given point on the Cartesian grid is calculated using the following formulae:

$$\Delta = \frac{180}{\pi * 6371}\sqrt{dx^2 + dy^2} \tag{B.1}$$

$$\alpha = \frac{180}{\pi}\arctan(\frac{dx}{dy}) \tag{B.2}$$

Δ is the angular distance between the two points, α is the azimuth of the point with respect to the station measured clockwise from north, dx and dy are the x and y components of the distance from the station to the point measured in the Cartesian coordinate system (Lay and Wallace, 1995). Then the latitude and longitude for that point on the sphere is calculated using the distance and azimuth using the following

equations:

$$lat_{point} = 90 - \arccos(\cos(90 - \Delta - lat_{station}) - \cos(lat_{station}) * \cos(90 - \Delta) * (1 - \cos(\alpha))) \tag{B.3}$$

$$lon_{point} = lon_{station} + \arctan(\frac{sin(\alpha) * \cos(90 - \Delta)}{\sin(90 - \Delta - lat_{station}) + \sin(lat_{station}) * \cos(90 - \Delta) * (1 - \cos(\alpha))}) \tag{B.4}$$

With the latitude and longitude of the point, the velocity can be interpolated from the spherical model.

Appendix C

Flattening Corrections

When flattening a three-dimensional model of velocity, a compensation must be made for the difference in the length of the ray path connecting two points on a sphere and the path connecting the same two points on a flat earth model. To compensate for the longer ray path in the Cartesian model, velocities must be slightly faster with depth than in the spherical model. Approximate flattening corrections were applied to the velocity model using the following formula.

$$v_{flattened}(i) = e^{\frac{z(i)}{6371}} * v_{original}(i) \tag{C.1}$$

where $v_{original}(i)$ is the ith velocity in the spherical model, $v_{flattened}(i)$ is the ith velocity in the Cartesian model, and z(i) is the depth of the original velocity (Biswas and Knopoff, 1970).

Appendix D

Comparison of GSEL and HYPOINVERSE

The widely used, one-dimensional earthquake location program HYPOINVERSE (Klein, 1978) was used to compute locations for three real events using the one-dimensional six layer model (Ran Zhou et al., 1995). The six layer model was chosen from a group of one-dimensional models after it returned the smallest residual normals for the three events discussed below. GSEL locates the events using travel time tables generated by HYPOINVERSE for the same one-dimensional model. For all three events, the resulting residual normal from the GSEL location is smaller than that from the HYPOINVERSE location. This confirms that the GSEL program is finding a better location in each case (where better means a more accurate data fit as measured by the residual normal). Differences in location can be seen in figures 4-6 and 4-7 where the location by HYPOINVERSE is marked with green circles and the locations by GSEL using the one-dimensional model are marked by red diamonds. GSEL is used for locating events because it returns a smaller residual normal than HYPOINVERSE for one-dimensional models and because it has the capability of locating events in three-dimensional models.

Bibliography

[1] Bernard, M., D. Reiter, S. Rieven, W. Rodi, and C. Vincent (1999). Development of a 3-D model for improved seismic event location in the Pakistan/India region, *Proceedings of the 21st Seismic Research Symposium: Technologies for Monitoring the Comprehensive Nuclear-Test-Ban Treaty*, September 21-24, 1999, 1, 374-382.

[2] Biswas, N. N. and L. Knopoff (1970). Exact earth-flattening calculations for Love waves, *Bull. of the Seis. Soc. Am.*, 60, 1123-1137.

[3] Buland, R. (1976). The mechanics of locating earthquakes, *Bull. of the Seis. Soc. of Am.*, 66 (1), 173-187.

[4] Burchfiel, B. C., Z. chen, Y. Liu, L. Royden (1995). Tectonics of the Longmen Shan and adjacent regions, Central China, *Int. Geol. Review*, 37 (8), 611-735.

[5] Dreger, D., R. Uhrhammer, M. Pasyanos, J. Franck, and B. Romanowicz (1998). Regional and Far-Regional Earthquake Locations and Source Parameters using Spare Broadband Networks: A Test on the Ridgecrest Sequence, *Bull. of Seis. Soc. of Am.*, 88 (6), 1353-1362.

[6] Eberhart-Phillips, D. and A. Michael (1993). Three-Dimensional Velocity Structure in the Parkfield Region, Central California, *Journal of Geophysical Research*, 98(B9), 15,737-15,758.

[7] Efron, B. and G. Gong (1983). A Leisurely Look at the Bootstrap, the Jackknife, and Cross-Validation, *The American Statistician*, 37 (1), 36-48.

[8] Flinn, E. A. (1965). Confidence Regions and Error Determinations for Seismic Event Location, *Reviews of Geophysics*, 3 (1), 157-185.

[9] Geiger, L. (1910). Herdbestimmung bei Erdbeben aus den Ankunftzeiten, *K. Gessell. Wiss. Goett.*, 4, 331-349.

[10] Julian, B. R. and D. Gubbins (1977). Three-Dimensional Seismic Ray Tracing, *J. Geophysics*, 43, 95-113.

[11] Kimura, G., M. Takahashi and M. Kono (1990). Mesozoic collision-extrusion tectonics in eastern Asia. In: M. Kono and B. C. Burchfiel (Editors), Tectonics of eastern Asia and Western Pacific Continental Margin. *Tectonophysics*, 181, 15-23.

[12] Klein, F. W. (1978). *Hypocenter Location Program: HYPOINVERSE*, Open-file Report 78-694, Department of Interior U. S. Geological Survey.

[13] Lay, T. and T. Wallace (1995). *Modern Global Seismology*:Boston, Academic Press, pp.135-136.

[14] Li Fu-tian, Wu Hua, Liu Jian-hua, Hu Ge, Li Qiang and Qu Ke-xin (1990). 3-D velocity images beneath the Chinese continent and adjacent regions, *Geophys. J. Int.*, 101, 379-394.

[15] Li, S., and W. D. Mooney (1998). Crustal structure of China from deep seismic sounding profiles, *Tectonophysics*, 288, 105-113.

[16] Liu Ruifeng, Chen Peishan, and Li Qiang (1993). Three-dimensional velocity images in Yunnan and its neighboring district, *Acta Seismologica Sinica*, 15 (1), 61-67.

[17] Lomax, A., et al. (2000). *NonLinLoc*
`http://iapetus.unice.fr/ lomax/nlloc/`

[18] McNamara, D. E., W. R. Walters, T. J. Owens, and C. J. Ammon (1997). Upper mantle velocity structure beneath the Tibetan Plateau from Pn travel time tomography, *J. of Geophys. Research*, 102 (B1), 493-505.

[19] Moser, T. J. (1991). Shortest path calculation of seismic rays, *Geophysics*, 56(1), 59-67.

[20] Ou, Q. and D. Deng (1995). Advances of geophysical prospecting for petroleum in marine carbonate areas of the upper Yangtze region, southern China, *Geophysics*, 60 (5), 1295-1305.

[21] Podvin, P. and I. Lecomte (1991). Finite difference computation of traveltimes in very contrasted velocity models: a massively parallel approach and its associated tools, *Geophys. J. Int.*, 105, 271-284.

[22] Ren Jishun, Jiang Chunfa, Zhang Zhengkun, and Qin Deyu under the direction of Huang Jiqing (1987). *Geotectonic Evolution of China*: New York, Springer-Verlag, pp. 41-81, 108-109.

[23] Sambridge, M. S. (1999). Geophysical inversion with a neighbourhood algorithm-I. Searching a parameter space, *Geophys. J. Int.*, 138, 479-494.

[24] Sambridge, M. S. and B. L. Kennett (1986). A novel method of hypocentre location, *Geophys. J. R. astr. Soc.*, 87 (2), 679-697.

[25] Um, J. and C. Thurber (1987). A fast algorithm for two-point seismic ray tracing, *Bull. of the Seis. Soc. of Am.*, 77 (3), 972-986.

[26] Vidale, J. E. (1990). Finite-difference calculation of traveltimes in three dimensions, *Geophysics*, 55 (5), 521-526.

[27] Wang Kai, and Yao Zhen-xing (1991). Upper mantle P velocity structure of Southern China, *Acta Geophysica Sinica*, 34 (3), 309-317.

[28] Wang Shangwen (ed.) (1983). *The petroleum geology of China*: Beijing, Petroleum Press, p 348.

[29] Xiong Shao-bai, Zheng Ye, Yin Zhou-xun, Zeng Xiao-xian, Quan You-li, and Sun Ke-zhong (1993). The 2-D structure and its tectonic implications of the crust in the Lijiang-Panzhihua-Zhehai region, *Acta Geophysica Sinica*, 36 (4), 434-443.

[30] Yin Zhou-xun and Xiong Shao-bai (1992). Explosion seismic study for the 2-D crustal structure in Xichang-Dukou-Muding region, *Acta Geophysica Sincia*, 35 (4), 451-458.

[31] Zeng Rongsheng, Zu Jieshou, Zhou Bing, Ding Zhifeng, He Zhengqing, Zhu Lupei, Luo Xun, and Sun Weigou (1992). Three-dimensional seismic velocity structure of the Tibetan Plateau and its eastern neighboring areas with implications to the model of collision between continents, *Acta Seismologica Sinia*, 14 (supp.), 523-533.

[32] Zhou, R., F. Tajima, and P. L. Stoffa (1995). Application of Genetic Algorithms to Constrain Near-Source Velocity Structure for the 1989 Sichuan earthquakes, *Bull. of the Seis. Soc. of Am.*, 85 (2), 590-605.